Journal of Power Sources 195 (2010) 1739–1746

Contents lists available at ScienceDirect

Journal of Power Sources

journal homepage: www.elsevier.com/locate/jpowsour

High capacitance B/C/N composites for capacitor electrodes synthesized by a simple method

Hidetaka Konno*, Teruhiko Ito, Mariko Ushiro, Koji Fushimi, Kazuhisa Azumi

Laboratory of Advanced Materials Chemistry, Graduate School of Engineering, Hokkaido University, Sapporo 060-8628, Japan

ARTICLE INFO

Article history:
Received 27 August 2009
Received in revised form
30 September 2009
Accepted 30 September 2009
Available online 9 October 2009

Keywords:
B/C/N composite
Polyacrylamide
Boric acid
B–N bond
Pseudo-capacitance

ABSTRACT

The B/C/N composites were synthesized by a very simple method, that is, carbonization at HTT = 800–1200 °C of the precursor prepared by drying a solution mixture of polyacrylamide and boric acid, followed by boiling in water to remove borate by-products. The amount of insoluble B species in the composite increased linearly from 4.8 to 18.6 mass% with raising HTT. The XRD and FT-IR revealed that turbostratic h-BN started to form at around 1000 °C as a by-product. By XPS, major B and N components in the composite were >B–N< bond, C–B–O type B, pyridinic N, pyrrolic N, and quaternary N. A fraction for >B–N< bond including h-BN in the total B or N components increased with raising HTT and it exceeded 50 at% between 900 and 1000 °C. It was suggested that in the composites formed at HTT > 1000 °C the amounts of h-BN increased, leading to reduction in other B and N components. The S_{BET} was almost unchanged up to 1000 °C, 410–420 $m^2 g^{-1}$. Large and broad redox peaks arisen from plural reactions appeared in the cyclic voltammogram (CV) measured in 1 mol dm^{-3} H_2SO_4 for the composites formed at HTT ≤ 1000 °C. These peaks disappeared in 1 mol dm^{-3} solutions of Na_2SO_4 and Li_2SO_4. By comparing CV with that for C/N composite formed from PAA by the MgO template method, the pseudo-capacitance owing to reactions of >B–N< and C–B–O components with protons was found to be added to commonly observed pseudo-capacitance for nitrogen-doped carbons. The capacitances for the composites formed at 850–950 °C exceeded 300 F g^{-1} at 2 mV s^{-1} in the acid electrolyte and the retention at 50 mV s^{-1} was 78–80%. The shape of CV in the neutral electrolytes was trapezoid and the current density increased with lowering potential, suggesting adsorption and desorption of Na^+ and Li^+ ions. This was considered to be due to doped nitrogen, indicating the development of pseudo-capacitance. The capacitance per S_{BET} was 0.33–0.74 F m^{-2} and 0.17–0.32 F m^{-2}, larger for lower HTT, in the acid and neutral electrolytes, respectively.

1. Introduction

The energy density of the electrochemical capacitor using aqueous electrolyte is low due to low terminal voltage. This capacitor, however, is potentially beneficial to large installations for storage of surplus power and unsteady electricity in costs, safety, and lifetime, compared with the electric double layer capacitor (EDLC) using organic electrolyte. To compensate low terminal voltage, high capacitance electrodes are required. A variety of porous carbons are used for commercial EDLCs but it has been reported that a capacitance limit of the ideal porous carbon having slit pores is estimated to be 210 F g^{-1} (130 F cm^{-3}), when the capacitance arises only from the electric double layer [1]. This value is hardly achieved with the activated carbons prepared even by sophisticated processes and still it is insufficient for the above applications. Accordingly explorations into different electrode materials are proceeding mainly aiming at the development of pseudo-capacitance. In this category, doped carbons are one of the promising materials and of them nitrogen-doped carbons have received much attention [2–10]. The gain in capacitance by nitrogen doping is frequently attributed to redox reactions of the functional groups containing nitrogen (*e.g.* [6]), but the amounts of nitrogen in most of the nitrogen-doped carbons are insufficient to explain it. A few more rationales, such as improving wetness of the pore walls due to the formation of polar functional groups, increasing capacitance of the space-charge layer due to the increase in carrier concentration, and others [11], are proposed but it is difficult to estimate each contribution.

The nitrogen-doped carbons are readily formed by carbonization of organic compounds containing nitrogen, mainly polymers, but the nitrogen content, W_N, of formed carbons decreases markedly with increasing heat treatment temperature (HTT). In addition, subsequent activation process to increase the specific surface area, S_{BET}, drastically lowers W_N [2,5,7,9]. Accordingly, high level of W_N is ensured either by limiting HTT (*e.g.* [8]) or by post-treatment with compounds containing nitrogen (*e.g.* [9,10]).

* Corresponding author. Tel.: +81 11 706 7114; fax: +81 11 706 7114.

0378-7753/$ – see front matter © 2009 Elsevier B.V. All rights reserved.
doi:10.1016/j.jpowsour.2009.09.072

We have reported that when boron is added to the carbon precursors containing nitrogen, the decrease in W_N due to high HTT is significantly moderated with the formation of >B–N< bond in the basic structural unit, BSU, of carbon [12–14]. Nitrogen doping into the carbon hexagonal structure causes slight distortion of the hexagonal plane [15] and also imbalanced distribution of the net charges on carbon and nitrogen atoms in the plane [14,15]. The extent of uneven charge distribution becomes larger by the presence of >B–N< bond than the substituted nitrogen [14]. Expecting the beneficial effects by boron and nitrogen co-doping, we have synthesized B/C/N composites by carbonizing the complexes of *N*-methyl-D-glucamine and boric acid [16]. The composites showed maximum 250 F g^{-1} in 1 mol dm^{-3} H_2SO_4, which can stand comparison with the values for the boron and nitrogen co-doped porous carbons reported recently [17]. Our process is very simple compared with the reported one [17], but we found much simpler method since then. In the present work, B/C/N composites were synthesized just by carbonizing a mixture of polyacrylamide (PAA) and boric acid, and they showed much larger capacitance than the previous ones.

2. Experimental

The PAA was a commercial reagent (Aldrich, 50 mass% aqueous solution) and the average molecular mass of PAA was 10000. Based on the chemical structure, N/C mole ratio in PAA is 1/3 and W_N is 19.7 mass%. The carbon yield from PAA is around 20 mass% in a temperature range of 800–1200 °C [18]. Boric acid and the PAA solution were dissolved into hot water at a mass ratio of PAA/H_3BO_3 = 3/7, then the solution was evaporated to dryness at 90 °C. Thus formed powder precursor was heated at 300 K h^{-1} to a set temperature in a range of 800–1200 °C and kept for 1 h at each temperature in a flow of pure nitrogen. The products were ground and boiled in water to dissolve borate by-products, filtrated, then dried at 90 °C for 24 h. Hereafter, formed B/C/N composites are referred to as PAAB-900 and so on with HTT in Celsius. Additionally carbonization in pure argon was also carried out to examine the effect of atmosphere, and a symbol "(Ar)" is added at the end, such as PAAB-1200(Ar).

The products were characterized by X-ray diffraction (XRD; Rigaku RAD-X RINT2000, Cu Kα, 40 kV, 20 mA), nitrogen adsorption/desorption measurements at 77 K (BEL Belsorp-mini), X-ray photoelectron spectroscopy (XPS; Shimadzu ESCA-3200, Mg Kα, 240 W), and infrared spectroscopy (FT-IR; Nicolet AVATAR 320 FT-IR, diamond crystal ATR method). Boron content was measured by inductively coupled plasma atomic emission spectrometry (ICP-AES; SII SPA 3000) after alkaline melting in a platinum crucible.

The composites were fabricated to working electrodes by mixing with acetylene black and PTFE, 10 mass% each, and pressing onto titanium mesh. The electrode capacitance, C_M in F g^{-1}, was evaluated by integrating a cyclic voltammogram (CV) measured using a three electrode cell, with Pt counter and SCE reference electrodes, in 1 mol dm^{-3} solutions of H_2SO_4, Na_2SO_4, and Li_2SO_4. The potential range was −0.2 to +0.8 V vs. SCE in 1 mol dm^{-3} H_2SO_4, and −0.4 to +0.6 V in the latter two. The potential scan rate, *r*, was 2–50 mV s^{-1}. Chronopotentiometric measurements were carried out at 0.5 and 1 A g^{-1} in 1 mol dm^{-3} H_2SO_4 using the three electrode cell described above. The value of C_M was calculated with respect to the total mass of composite (the active material).

3. Results

3.1. Characterization of B/C/N composites

The XRD patterns of B/C/N composites are shown in Fig. 1. In the patterns of PAAB-800 to PAAB-1000 only broad 002 and faint 10 peaks of carbon are observed, but in the patterns of PAAB-1100 and PAAB-1200 an additional sharp 002 peak of rhombohedral boron nitride is distinguished. The formation of boron nitride phase is confirmed by the narrow range XRD pattern of PAAB-1200 (an inset in Fig. 1). The patterns resemble h-BN (JCPDS 45-1171) but strictly speaking they are turbostratic h-BN. The FT-IR spectra give more detailed information as shown in Fig. 2. In the h-BN phase, vibrational modes absorb at around 1380 and 760 cm^{-1}, corresponding to the in-plane B–N stretching and out-of-plane B–N–B bending, respectively [19]. The spectrum of a reagent h-BN measured in the present work coincides with this. The spectra in Fig. 2 clearly indi-

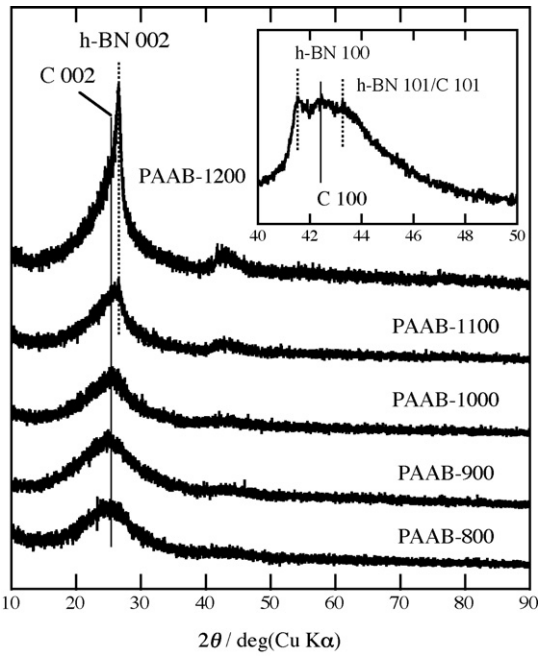

Fig. 1. XRD patterns of B/C/N composites. An inset is a narrow range pattern for PAAB-1200.

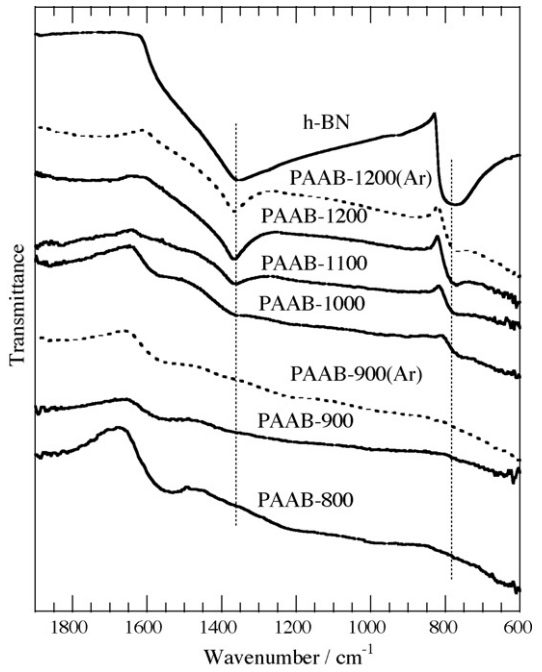

Fig. 2. FT-IR spectra for B/C/N composites. The spectra for the composites formed in an argon atmosphere are shown by broken lines.

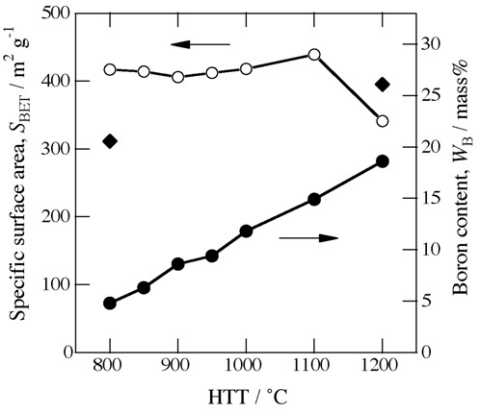

Fig. 3. Boron content, W_B (filled symbols) and the specific surface area, S_{BET} (open symbols) as a function of HTT. A symbol (♦) indicates W_B for the composites before boiling in water.

cate that turbostratic h-BN phase starts to form as a by-product at around 1000 °C. As the spectra do not change by the atmosphere used, N_2 or Ar, a source of nitrogen is PAA.

Boron content, W_B, and the specific surface area, S_{BET}, are shown as a function of HTT in Fig. 3, where the values of W_B for PAAB-800 and PAAB-1200 before boiling in water are also indicated. The total boron content before the boiling is not greatly different by HTT, but W_B after the boiling increases linearly with raising HTT. This indicates that soluble borate species are converted into insoluble ones, namely turbostratic h-BN and boron species incorporated into the composite, with raising HTT. Since W_B is considerably large, conventional elemental analysis was unsuccessful due to incomplete combustion. The S_{BET} is almost unchanged up to 1000 °C, 410–420 m^2 g^{-1}, and slightly increases at 1100 °C, then decreases to 340 m^2 g^{-1} at 1200 °C. This dependence on HTT is parallel to that of the pore size distribution calculated by BJH method as shown in Fig. 4. The distributions for PAAB-800 to PAAB-1000 are practically the same and micropores are predominant, though the distributions for R_p < 1 nm were not determined due to the limitation of the instrument used. Development of mesopores is distinct for PAAB-1100 and much larger mesopores increase for PAAB-1200, and it is probably related to the formation of h-BN by-product (Figs. 1 and 2).

For PAAB-900 and PAAB-1200, XPS spectra of C 1s, B 1s, and N 1s are shown in Fig. 5. The C 1s spectra were practically the same for all composites (Fig. 5(a)). Here, the background lines were drawn by the empirical Shirley method, and the peak separation was carried out by assigning an identical peak profile (the same FWHM and Gaussian/Lorentzian mixing ratio) to each component in one spectrum. There were five types of C component and they were numbered from lower binding energy, E_B: peak I, E_B[C 1s] = 284.5–284.6 eV; peak II, E_B[C 1s] = 286.0–286.1 eV; peak III, E_B[C 1s] = 287.7–287.9 eV; peak IV, E_B[C 1s] = 288.9–289.3 eV; and peak V, E_B[C 1s] = 290.6 eV. These components are assigned to the following carbon species in carbon materials: peak I, turbostratic carbon; peak II, C–OH (286.1 eV [20,21]); peak III, C=O (287.6 eV [20], 288.2 eV [21]); peak IV, C(=O)OH (289.1 eV [20], 288.8 eV [21]); and peak V, carbonate or shake-up satellite (290.6–290.7 eV [20,21]). As E_B for turbostratic carbon was 284.5–284.6 eV, E_B was not corrected. In the case of granular samples, the quality of XPS spectrum is critically affected not only by the content, but also by the surface morphology and often by crystallinity. Accordingly, FWHM of certain component changes sample by sample. There were three types of B component and they were numbered from lower E_B (Fig. 5(b)): peak I, E_B[B 1s] = 190.5–190.7 eV; peak II, E_B[B 1s] = 191.6–191.8 eV; and peak III, E_B[B 1s] = 192.8–193.1 eV. The peak III was not distinguished for PAAB-800 and PAAB-900 (Fig. 5(b)). Substituted boron in BSU (E_B[B 1s] ~ 188 eV [12,14]) was not observed. There were five types of N component and they were also numbered from lower E_B (Fig. 5(c)): peak I, E_B[N 1s] = 398.3–398.4 eV; peak II, E_B[N 1s] = 398.7–398.9 eV; peak III, E_B[N 1s] = 399.9–400.4 eV; peak IV, E_B[N 1s] = 401.5–401.8 eV; and peak V, E_B[N 1s] = 403.9–404.1 eV. All five N components were observed for PAAB-800 and PAAB-900, but peaks IV and V were not distinguished for PAAB-1100 and PAAB-1200 (Fig. 5(c)). The peak I of B and N components is assigned to >B–N< bond present in BSU [12,14] or boron nitride [22]. The peaks II and III of B component are assigned to C–B–O type [12,14] and oxide (and/or hydroxide) [14,22], respectively. The C 1s peak for C–B–O type component is difficult to distinguish it from turbostratic carbons, because the donation of electrons from boron atom is limited due to B–O bonding. The peaks II–V of N component are assigned to the following nitrogen species in carbon materials: peak II, pyridinic N (398.3 eV [23], 398.7 eV [24]); peak III, pyrrolic N (400.1 eV [23], 400.3 eV [24]); peak IV, quaternary N (401.3 eV [23], 401.4 eV [24]); and peak V, N-oxide (402–405 eV [23], 403.1 eV [25]). The N II–V components are generally observed in nitrogen-doped carbons with various intensities [3,5,6,10,26]. In the case of granular and porous carbon materials, estimation of composition by XPS is meaningless, though ratios of different components in one spectrum are possible to calculate based on the peak separation. Accordingly quantitative comparison between the composites is not possible, but for overview of the changes in the surface composition by HTT, the atomic fraction of each component and the peak intensity ratios by area, I[B 1s]/I[C 1s] and I[N 1s]/I[C 1s], were plotted against HTT as shown in Fig. 6. The C V component (carbonate or shake-up satellite) and N V component (N-oxide) were omitted in Fig. 6 because of low intensities, and accessory broken lines are only used as a visual aid. It is plain from Fig. 6 that the proportion of C components is nearly the same for all composites. There may be two reasons that the total fraction of the surface functional groups, C–OH, C=O, and C(=O)OH, (C II + C III + C IV) does not change very much by HTT: one is that the measured proportion is intrinsic to these composites, and the other the results were brought about by the leveling effect due to boiling in water. The latter reason, however, is unlikely because it is commonly observed that the boiling in distilled water does not alter or produce significant amounts of these functional groups on carbon. Fig. 6 reveals that a fraction for >B–N< bond (B I and N I) increases with raising HTT and it exceeds 50 at% between 900 and 1000 °C. As described above, h-BN by-product starts to form in the composites at around 1000 °C, and so the number of >B–N< bonds in BSU may be reduced at around 1000 °C and higher HTT. As secondary information from Fig. 6, it seems that the trend of I[B 1s]/I[C 1s] is very similar to W_B in Fig. 3. Accordingly, it may be allowed to say that the surface boron concentration increases with

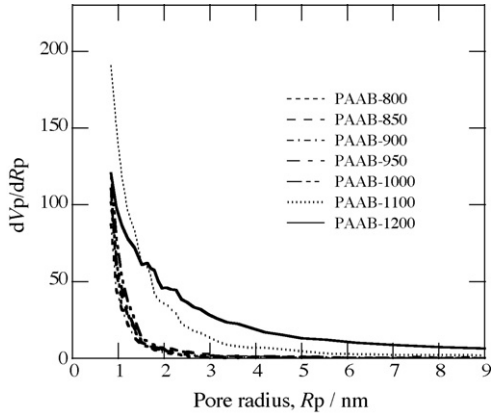

Fig. 4. Pore size distributions by BJH method.

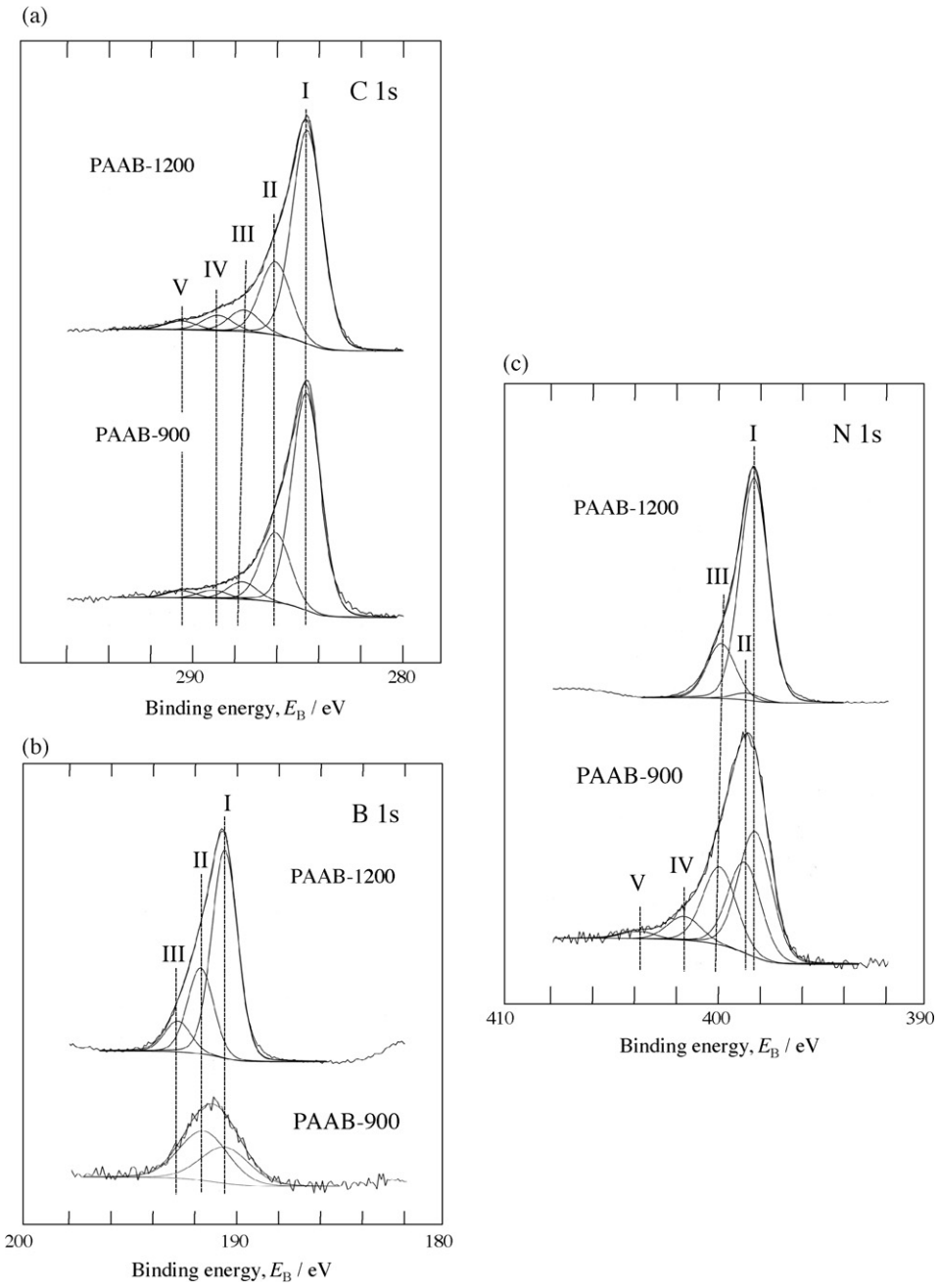

Fig. 5. XPS spectra of (a) C 1s, (b) B 1s, and (c) N 1s for PAAB-900 and PAAB-1200.

raising HTT, which leads to the consequence that the surface nitrogen concentration (I[N 1s]/I[C 1s]) is not markedly affected by HTT, at least below 1200 °C. Although the nitrogen content, W_N, was not obtained by the elemental analysis, the results of XPS analysis imply that in a range of HTT < 1000 °C the total amounts of N components including >B–N< bond is probably larger than the amounts of B II component (C–B–O type). Note that O 1s spectra do not give useful information, since the composites were obtained after boiling in water.

3.2. Capacitive performance of B/C/N composites

The CVs of 10th cycle in 1 mol dm^{-3} H_2SO_4 at r = 2 mV s^{-1} for B/C/N composites are shown in Fig. 7. The current density, i_M in A g^{-1}, increases very slightly from PAAB-800 to PAAB-900, and then decreases from PAAB-900 to PAAB-1200. The CVs for PAAB-850 and PAAB-950 are identical to that for PAAB-900, and absent from Fig. 7. The shape of CVs clearly indicates that a few current peaks due to redox reactions overlap each other in the middle part of CVs. The top part of CVs locates at around 0.35 V (anodic) and 0.3 V (cathodic) vs. SCE, and a shoulder at 0–0.2 V vs. SCE except for PAAB-1200. The shoulder is undistinguishable for PAAB-1200. As shown in Fig. 8, these peaks disappear in 1 mol dm^{-3} solutions of Na_2SO_4 and Li_2SO_4, and the shape of CV is independent of cation species in the neutral electrolytes. Therefore, large i_M in the middle part of CVs in the acid electrolyte is originated from the redox reactions related to protons. These peaks are often attributed to redox reactions of the functional groups containing oxygen on the carbon surface. It has been reported that C(=O)OH group develops peaks at about 0.4 V (anodic) and 0.3 V (cathodic) vs. Ag/AgCl, whereas C-OH group does not give distinct peaks in 1 mol dm^{-3} H_2SO_4 [27]. Although the potentials of the top parts of CVs in Fig. 7 are similar to

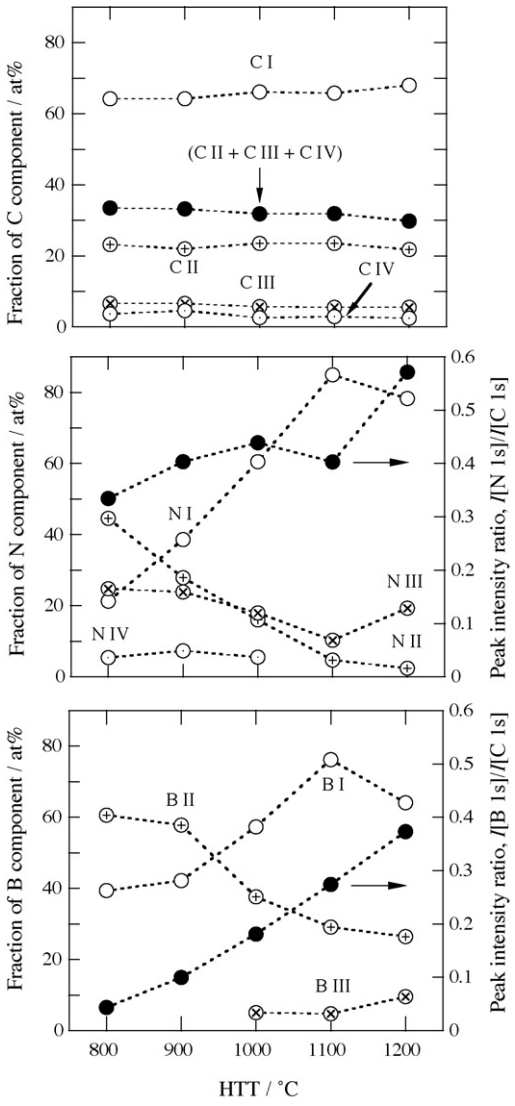

Fig. 6. Fraction of B and N components by XPS, and the peak intensity ratios of I[B 1s]/I[C 1s] and I[N 1s]/I[C 1s]. Here, N V component was omitted because of small values. See text for the detail of each component.

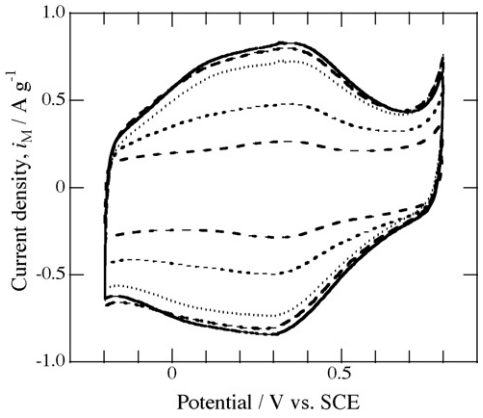

Fig. 7. Cyclic voltammograms for PAAB-800 (– – –), PAAB-900 (↓), PAAB-1000 (·····), PAAB-1100 (· · · ·) and PAAB-1200 (- - -) in 1 mol dm^{-3} H_2SO_4 at r = 2 mV s^{-1}.

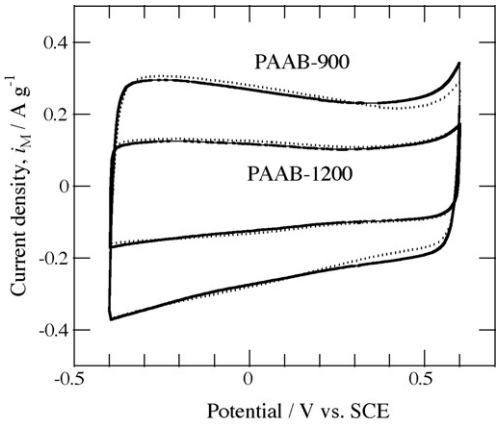

Fig. 8. Cyclic voltammograms for PAAB-900 and PAAB-1200 in 1 mol dm^{-3} Na_2SO_4 (↓) and 1 mol dm^{-3} Li_2SO_4 (·····) at r = 2 mV s^{-1}.

the reported potentials (note that the reference electrode is different), a substantial contribution of above carbonaceous functional groups to i_M is unlikely in the case of B/C/N composites. It is simply deduced from markedly decreasing i_M for the composites formed at HTT > 1000 °C (Fig. 7), while the proportions of C–OH and C(=O)OH groups do not change by HTT (Fig. 6). It is notable that the decrease of i_M is not attributed to the difference in the number density of functional groups on the surface, since S_{BET} is comparable to each other (Fig. 3) and much larger pores are present in PAAB-1100 and PAAB-1200 (Fig. 4).

For all composites, CV held a shape similar to that at r = 2 mV s^{-1} up to r = 20 mV s^{-1}, but distorted at r = 50 mV s^{-1}. The capacitance calculated from CV, C_M, is shown in Fig. 9 as a function of r. The composites formed at HTT = 800–1000 °C present nearly equivalent performance in each electrolyte, except for PAAB-1000 in 1 mol dm^{-3} H_2SO_4. The values of C_M for PAAB-850 to PAAB-950 at r = 2 mV s^{-1} exceed 300 F g^{-1} in 1 mol dm^{-3} H_2SO_4 and fairly good retention is achieved at r = 50 mV s^{-1}, 78–80% (Fig. 9(a)). This performance is superior to the boron and nitrogen co-doped porous carbons prepared by the complicated procedure [17]. The performance in 1 mol dm^{-3} Na_2SO_4 (Fig. 9(b)) and 1 mol dm^{-3} Li_2SO_4 (Fig. 9(c)) does not make much difference. The values of C_M for PAAB-800 to PAAB-1000 in the neutral electrolytes are considerably large despite moderate values of S_{BET}. This is discussed later together with lower retention of C_M against r.

The specific capacitance normalized by the specific surface area, $C_A = C_M/S_{BET}$, at r = 2 mV s^{-1} is plotted against HTT in Fig. 10. The values of C_A for the composites formed at HTT ≤ 1000 °C are comparable to or larger than the values of nitrogen-doped carbons in acidic electrolytes [3–6,9,10], and larger than the values of EDLC, 0.05–0.15 F m^{-2}.

Chronopotentiographs at 0.5 and 1 A g^{-1} for PAAB-900 are shown in Fig. 11. The potential changes are not neatly linear probably due to the pseudo-capacitance and also by IR drops. Estimation of capacitance from these curves is not simple, but the time scale suggests that C_M may be much larger than 200 F g^{-1} at both current densities.

4. Discussion

Simply carbonized PAA has very small specific surface area, S_{BET} < 10 m^2 g^{-1}. Further, we found that carbons derived from a mixed powder of poly(vinyl alcohol) and boric acid were S_{BET} < 50 m^2 g^{-1}, while those derived from glucose–borate complexes had S_{BET} of 850–1360 m^2 g^{-1} with micropores, after removing borate by-products in boiling water [28]. It indicates that chemical interactions between the carbon precursor and borate ions are essential to

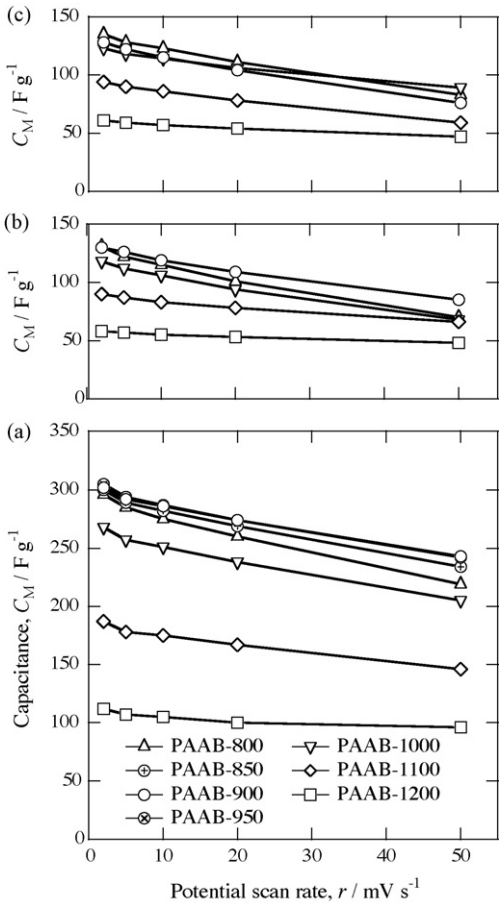

Fig. 9. Capacitance, C_M, in (a) 1 mol dm^{-3} H_2SO_4, (b) 1 mol dm^{-3} Na_2SO_4, and (c) 1 mol dm^{-3} Li_2SO_4 as a function of potential scan rate, r.

develop pores leading to large S_{BET}, that is, infinitesimal clusters of borate species must be formed in the products after pyrolysis. In the present case, it is probable that the precursor formed from a mixed solution of PAA and boric acid by evaporation to dryness at 90 °C is not a simple mixture of them but something complex-like. Moderately large values of S_{BET} support this (Fig. 3). The N/B mole ratio in the starting solution is approximately 10/27. The ratio of soluble boron species to insoluble ones at HTT = 800 °C (Fig. 3) suggests that

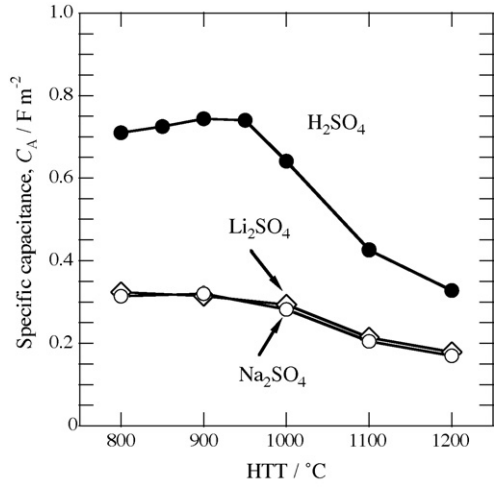

Fig. 10. Specific capacitance, $C_A = C_M/S_{BET}$, in 1 mol dm^{-3} solutions of H_2SO_4, Na_2SO_4, and Li_2SO_4 as a function of HTT.

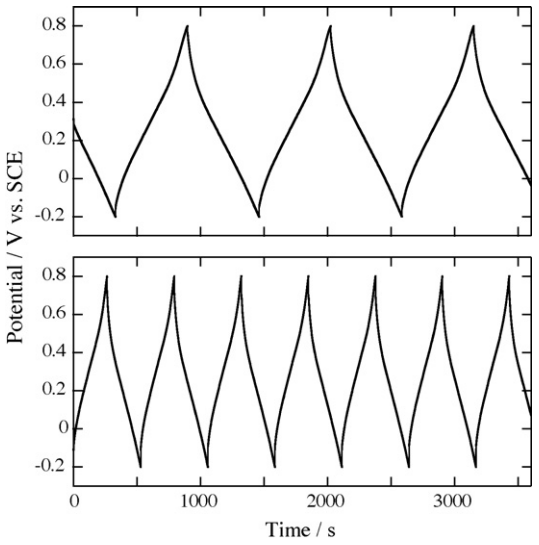

Fig. 11. Chronopotentiographs of PAAB-900 at 0.5 A g^{-1} (upper) and 1 A g^{-1} (lower) in 1 mol dm^{-3} H_2SO_4.

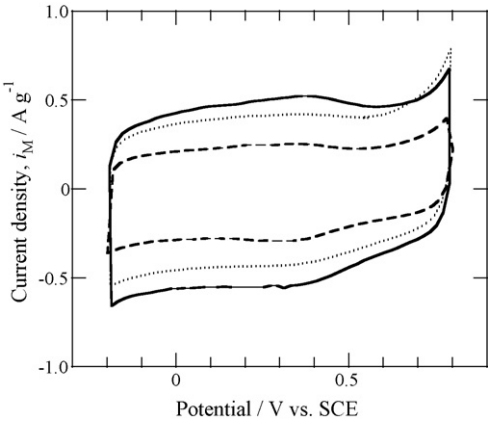

Fig. 12. Cyclic voltammograms for PAA-800(MgO) (·····), PAA-900(MgO) (↓), and PAA-1000(MgO) (– – –) in 1 mol dm^{-3} H_2SO_4 at r = 2 mV s^{-1}.

the amounts of boric acid in the starting solution may be reduced, but it might decrease S_{BET} according to the above pore-formation scheme.

As described in Section 3.2, the contribution of carbonaceous functional groups to large redox current in the sulfuric acid electrolyte (Fig. 7) is insignificant. Further, it is recognized that the pseudo-capacitance by nitrogen doping does not appear as prominent redox peaks [2–6,8,10]. For comparison, CVs for C/N composites derived from PAA by MgO template method [26] are presented in Fig. 12: experimental conditions are exactly the same as Fig. 7. Hereafter the composites are referred to as PAA-800(MgO) and so on, and some properties of them are summarized in Table 1. These C/N composites contain the same types of N component as B/C/N composites in different proportions. It is evident from the

Table 1
Properties of PAA carbonized by MgO template method [26] (*Name codes*: PAA-HTT(MgO)).

HTT (°C)	W_N (mass%)	S_{BET} (m^2 g^{-1})	C_M (F g^{-1})[a]	C_A (F m^{-2})[a]
800	10.1	498	196	0.394
900	8.1_6	740	234	0.316
1000	3.5_7	943	119	0.126

[a] From cyclic voltammograms at 2 mV s^{-1} in 1.0 mol dm^{-3} H_2SO_4.

values of W_N and C_A in Table 1 that the pseudo-capacitance due to doped-nitrogen is contributing to C_M of PAA-800(MgO) and PAA-900(MgO). The PAA-800(MgO) may be used as a reference on the grounds that S_{BET} is not largely different from the values for B/C/N composites (Fig. 3). In a potential region of −0.2 to +0.6 V vs. SCE, the values of i_M for PAAB-800 to PAAB-1000 (Fig. 7) are much larger than i_M for PAA-800(MgO) but a jump in i_M at the lower potential end is not so different. This suggests that the contribution from the doped-nitrogen (N II–IV) is at equivalent level for both types of composites, and that W_N for B/C/N composites is assumed to be more than 10 mass% taking >B–N< component into consideration (Fig. 6). Consequently, extra sources of pseudo-capacitance have to be C–B–O (B II) and >B–N< (B I and N I) components. The mechanism of redox reactions between these components and protons, however, is complicated and unknown at present, because the information on organoboron chemistry in aqueous media is lacking compared with that in organic ones.

At higher HTT, the formation of h-BN by-product reduces the doped-boron and nitrogen in the composites, in addition to the decrease of N components (N II–V) by pyrolysis (see [8] and Table 1, for example). Further, h-BN is an insulator and has very low dielectric constant. Thus, the decreased C_M for PAAB-1100 and PAAB-1200 (Figs. 7 and 9) is attributable to all these reasons. The shape of CV for PAAB-1100, however, has still similar features as B/C/N composites formed at lower HTT and $C_A = 0.426\ F\ m^{-2}$ (Fig. 10), and so the same scheme of pseudo-capacitance may be developed in this composite. For PAAB-1200, the shoulders of CV at 0–0.2 V vs. SCE are undistinguishable but broad peaks remain at around 0.35 V (anodic) and 0.3 V (cathodic) vs. SCE, and $C_A = 0.328\ F\ m^{-2}$ (Fig. 10). This C_A is larger than that for PAA-900(MgO) (Table 1), suggesting considerable contribution of pseudo-capacitance. As oxygen content generally decreases with raising carbonization temperature, there is a possibility that disappearance of shoulder peaks is related to C–B–O components. The value of W_B (Fig. 3) and a fraction of C–B–O type (B II) by XPS (Fig. 6), however, do not stand for this. As the cause of disappearance of shoulders, decrease in >B–N< bonds is not yet screened out. Obviously, it is not due to S_{BET}, because the reduction in S_{BET} is about 20% (Fig. 3) and the pore size distribution is more favorable to the electrochemical reactions than that of others (Fig. 4).

In the neutral electrolytes, i_M increased with lowering potential, and it was prominent for the composites formed at lower HTT (Fig. 8) with $C_A = 0.17–0.32\ F\ m^{-2}$ (Fig. 10). This suggests adsorption and desorption of Na^+ and Li^+ ions, leading to the increment of pseudo-capacitance. The shape of CV resembles that for nitrogen-enriched carbons in 6 mol dm^{-3} KOH solution [29] and it has been explained as pseudo-capacitive interactions between cations and the nitrogen atoms of carbon, though detailed background was not given [6,29]. It was reported that alkali ions in aqueous solutions adsorb into pores of carbon materials together with sizable hydration sheath [30]. A scale of ionic effective dimensions was estimated to be 0.362 nm < K^+ < Na^+ < Li^+ < 0.421 nm [30], which is slightly different from Stokes diameters, K^+: 0.26 nm, Na^+: 0.36 nm, and Li^+: 0.48 nm. With the present composites meaningful difference of performance between Na^+ and Li^+ ions was not recognized (Figs. 8 and 9), therefore the lower limit of effective pore diameter for the composites should be close to the larger side of above scale. The retention of C_M against r in the neutral electrolytes is slightly lower than the retention in the acid electrolyte for the composites formed at HTT ≤ 1000 °C (Fig. 9). It leads to the consequent that there are micropores, which affect the migration of hydrated Na^+ and Li^+ ions, in these composites. Naturally, better retention of C_M for PAAB-1100 and PAAB-1200 in all electrolytes is resulted from the presence of mesopores (Fig. 4).

In conclusion, large C_M of B/C/N composites is owing to the pseudo-capacitance developed by C–B–O and >B–N< components in addition to the doped-nitrogen (N II–IV). To keep high content of nitrogen and boron without forming the h-BN by-product, HTT of around 900 °C is favorable to the present precursor.

5. Summary

The B/C/N composites (PAAB-800 to PAAB-1200) were synthesized by a very simple method, that is, the precursor prepared by drying a solution mixture of PAA and boric acid (mass ratio = 3/7) was carbonized at HTT = 800–1200 °C, followed by boiling in water to remove borate by-products. Capacitive performance was evaluated mainly by the cyclic voltammetry in 1 mol dm^{-3} solutions of H_2SO_4, Na_2SO_4 and Li_2SO_4. The results are summarized as follows:

(1) The amount of insoluble boron species in the composite increased linearly from 4.8 to 18.6 mass% with raising HTT. The XRD and FT-IR revealed that turbostratic h-BN started to form at around 1000 °C as a by-product.
(2) By XPS, major B and N components in the composite were >B–N< bond, C–B–O type B, pyridinic N, pyrrolic N, and quaternary N. A fraction for >B–N< bond including h-BN increased with raising HTT and it exceeded 50 at% between 900 and 1000 °C. It was suggested that in the composites formed at HTT > 1000 °C the amounts of h-BN increased, leading to reduction in other B and N components.
(3) The S_{BET} was almost unchanged up to 1000 °C, 410–420 m^2 g^{-1}, and slightly increased at 1100 °C, then decreased to 340 m^2 g^{-1} at 1200 °C. This dependence on HTT was parallel to that of the pore size distribution. The distributions for PAAB-800 to PAAB-1000 were practically the same and micropores were predominant. Development of mesopores was distinct for PAAB-1100 and much larger mesopores increased for PAAB-1200.
(4) Large and broad redox peaks arisen from plural reactions appeared in CV measured in the acid electrolyte for the composites at HTT ≤ 1000 °C. These peaks disappeared in the neutral electrolytes. By comparing CV with that for C/N composite formed from PAA by the MgO template method, the pseudo-capacitance owing to reactions of >B–N< and C–B–O components with protons was found to be added to commonly observed pseudo-capacitance for nitrogen-doped carbons.
(5) The capacitances for PAAB-850 to PAAB-950 at $r = 2$ mV s^{-1} exceeded 300 F g^{-1} in 1 mol dm^{-3} H_2SO_4 and fairly good retention was achieved at $r = 50$ mV s^{-1}, 78–80%.
(6) The shape of CV in the neutral electrolytes was trapezoid and the current density increased with lowering potential, suggesting adsorption and desorption of Na^+ and Li^+ ions. This was considered to be due to doped nitrogen, indicating the development of pseudo-capacitance.
(7) The capacitance per S_{BET} was 0.33–0.74 F m^{-2} and 0.17–0.32 F m^{-2}, larger for lower HTT, in the acid and neutral electrolytes, respectively.

Acknowledgement

A part of the present work was supported by the Grant-in-Aid for Scientific Research (B) from JSPS (No. 18350102).

References

[1] S. Shiraishi, J. Jpn. Inst. Energy 81 (2002) 788–798.
[2] K. Jurewicz, K. Babel, A. Ziólkowski, H. Wachowska, M. Kozlowski, Fuel Process. Technol. 77–78 (2002) 191–198.
[3] K. Jurewicz, K. Babel, A. Ziólkowski, H. Wachowska, Electrochim. Acta 48 (2003) 1491–1498.
[4] M. Kodama, J. Yamashita, Y. Soneda, H. Hatori, S. Nishimura, K. Kamegai, Mater. Sci. Eng. B 108 (2004) 156–161.

[5] G. Lota, B. Grzyb, H. Machnikowska, J. Machnikowski, E. Frakowiak, Chem. Phys. Lett. 404 (2005) 53–58.
[6] D. Hulicova, J. Yamashita, Y. Soneda, H. Hatori, M. Kodama, Chem. Mater. 17 (2005) 1241–1247.
[7] Y.J. Kim, Y. Abe, T. Yanagiura, K.C. Park, M. Shimizu, T. Iwazaki, S. Nakagawa, M. Endo, M.S. Dresselhaus, Carbon 45 (2007) 2116–2125.
[8] M. Kodama, J. Yamashita, Y. Soneda, H. Hatori, K. Kamegawa, I. Moriguchi, Carbon 45 (2007) 1105–1107.
[9] K. Jurewicz, R. Pietrzak, P. Nowicki, H. Wachowska, Electrochim. Acta 53 (2008) 5469–5475.
[10] M. Seredych, D. Huricova-Jurcakova, G.Q. Lu, T.J. Bandosz, Carbon 46 (2008) 1475–1488.
[11] Y. Yamada, O. Tanaike, S. Shiraishi, TANSO No. 215 (2004) 285–294.
[12] H. Konno, H. Oka, K. Shiba, H. Tachikawa, M. Inagaki, Carbon 37 (1999) 887–895.
[13] H. Konno, K. Shiba, Y. Kaburagi, Y. Hishiyama, M. Inagaki, Carbon 39 (2001) 1731–1740.
[14] H. Konno, K. Shiba, H. Tachikawa, T. Nakahashi, H. Oka, M. Inagaki, Synthe. Met. 125 (2002) 189–196.
[15] M. Inagaki, H. Tachikawa, T. Nakahashi, H. Konno, Y. Hishiyama, Carbon 36 (1998) 1021–1025.
[16] H. Konno, T. Ito, K. Azumi, Proceedings of the Abstract O.4.6 of CESEP'07, Krakow, Poland, 2–6 September 2007.;
T. Ito, H. Konno, Proceedings of the Abstract P0063 of CARBON2008, Nagano, Japan, 13–18 July 2008.
[17] H. Guo, Q. Gao, J. Power Sources 186 (2009) 551–556.
[18] H. Konno, K. Fujita, H. Habazaki, M. Inagaki, TANSO No. 203 (2003) 113–113.
[19] N. Laidani, M. Anderle, R. Canteri, L. Elia, A. Luches, M. Martino, V. Micheli, G. Speranza, Appl. Surf. Sci. 157 (2000) 135–144.
[20] E. Desimoni, G.I. Casella, A. Morone, P.A.M. Sherwood, Surf. Interface Anal. 15 (1990) 627–634.
[21] H. Viswanathan, M.A. Rooke, P.A.M. Sherwood, Surf. Interface Anal. 25 (1997) 409–417.
[22] D. Briggs, M.P. Seah (Eds.), Practical Surface Analysis, second edition, John Wiley & Sons, Ltd., New York, 1990, p. 599.
[23] K. Stanczyk, R. Dziembaj, Z. Piwowarska, S. Witkowski, Carbon 33 (1995) 1383–1392.
[24] J.R. Pels, F. Kaptieijn, J.A. Moulijn, Q. Zhu, K.M. Thomas, Carbon 33 (1995) 1641–1653.
[25] S.R. Kelemen, M.L. Gorbaty, P.J. Kwiatek, Energy Fuels 8 (1994) 896–906.
[26] H. Konno, H. Onishi, N. Yoshizawa, K. Azumi, J. Power Sources 195 (2010) 667–673.
[27] H. Oda, A. Yamashita, S. Minoura, M. Okamoto, T. Morimoto, J. Power Sources 158 (2006) 1510–1516.
[28] T. Ito, M. Ushiro, K. Fushimi, K. Azumi, H. Konno, TANSO No. 239 (2009) 156–161.
[29] D. Hulicova, M. Kodama, H. Hatori, Chem. Mater. 18 (2006) 2318–2326.
[30] L. Eliad, G. Salitra, A. Soffer, D. Aurbach, J. Phys. Chem. B 105 (2001) 6880–6887.